Tuning the Postfocused Size of Colloidal Nanocrystals by the Reaction Rate: From Theory to Application

Sofie Abe,[†,‡] Richard Karel Čapek,[†,§,*] Bram De Geyter,[†,‡] and Zeger Hens[†,‡,*]

[†]Physics and Chemistry of Nanostructures, Ghent University, Krijgslaan 281-S3, 9000 Gent, Belgium and [‡]Center for Nano and Biophotonics, Ghent University, Belgium [§]Present address: Schulich Faculty of Chemistry, Russell Berrie Nanotechnology Institute, Technion, Haifa 32000, Israel

ABSTRACT

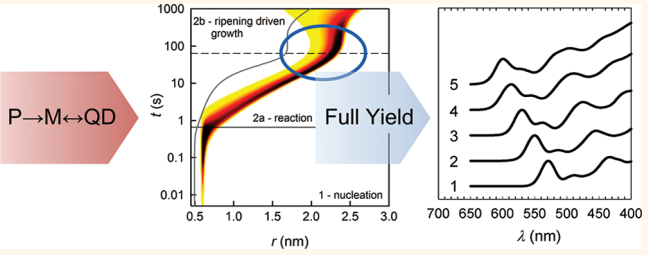

We show that adjusting the reaction rate in a hot injection synthesis is a viable strategy to tune the diameter of colloidal nanocrystals at the end of the size distribution focusing, *i.e.*, the postfocused diameter. The approach is introduced by synthesis simulations, which describe nucleation and growth of colloidal nanocrystals from a solute or monomer that is formed *in situ* out of the injected precursors. These simulations indicate that the postfocused diameter is reached at almost full yield and that it can be adjusted by the rate of monomer formation. We implement this size-tuning strategy using a particular CdSe quantum dot synthesis that shows excellent agreement with the model synthesis. After demonstrating that the reaction rate depends in first order on the Cd and Se precursor concentration, the proposed strategy of size control is explored by varying the precursor concentration. This enables the synthesis of colloidal nanocrystals with a predefined size at almost full yield and sharp size distributions. In addition, we demonstrate that the same tuning strategy applies to the synthesis of CdS quantum dots. This result is highly relevant especially in the context of reaction upscaling and automation. Moreover, the results obtained challenge the traditional interpretation of the hot injection synthesis, in particular the link between hot injection, burst nucleation, and sharp size distributions.

KEYWORDS: quantum dots · colloidal synthesis · reaction modeling · nucleation rate · postfocused size · size tuning · CdSe

Colloidal semiconductor nanocrystals or quantum dots (QDs) have opto-electronic properties that strongly depend on their size, structure, shape, and composition.[1−13] In addition, because they are colloidal particles sterically stabilized by ligands, wet chemical techniques can be used to functionalize them through ligand exchange,[14] and the formation of QD monolayers or thin films is possible by various wet-processing techniques such as spin coating, drop casting, layer-by-layer assembly,[15] or Langmuir−Blodgett deposition.[16,17] This unique combination of tunable opto-electronic properties and a suitability for wet chemical processing results in an exceptionally broad potential for applications, which extends from opto-electronic devices such as photodetectors,[18,19] LEDs,[20,21] and solar cells[22−24] to biolabeling[25] and sensing.[26]

For the characterization of their material properties and the development of these applications, the synthesis of QDs with sharp size distributions at desired mean sizes and high reaction yields is necessary. Until now two concepts, burst nucleation and focusing, are mainly applied in colloidal synthesis to achieve narrow size distributions.[27] In the hot injection synthesis, burst nucleation is supposedly achieved by the injection of reaction precursors at a high temperature, which leads to a high degree of supersaturation. This should result in a short nucleation event, which is stopped by the resulting drop of the supersaturation and the temperature. Next, it is assumed that nucleation is followed by a continuous growth at a lower temperature, thereby maintaining the initial sharp size distribution during the growth phase. In addition, it was shown that specific reaction conditions can even improve an initial size distribution.[28] This so-called focusing is based on the fact that when growth is limited by the diffusion of reagents to the QDs, the increase of the QD radius, r_{QD}, with time drops as $1/r_{QD}$. Since smaller particles grow faster than bigger particles under this condition, the initial particle size distribution narrows during growth.

The hot injection concept led to the development of synthesis schemes where QDs of different sizes are obtained by changing the reaction time.[2,29−35] Although highly successful, these procedures have an intrinsic

* Address correspondence to capek@technunix.technion.ac.il; Zeger.Hens@UGent.be.

Received for review May 27, 2011 and accepted December 1, 2011.

Published online December 01, 2011
10.1021/nn204008q

drawback: QDs with a size smaller than the size reached after focusing (a size referred to as the postfocused size d_{PF}), which often coincides with a reaction yield close to unity,[28] are only obtained at the expense of a reduced reaction yield and a suboptimal size dispersion. This is problematic when small QDs are targeted or in the context of reaction upscaling. Therefore, the development of strategies enabling the preparation of monodisperse batches of colloidal QDs with different diameters at the end of the reaction is of key importance. A number of literature examples indicate possible approaches in this respect. Various authors have shown for CdSe and CdS QDs synthesized in noncoordinating solvents that a decrease of the concentration of carboxylic or phosphonic acids leads to a reduction of the QD diameter.[36−40] Alternatively, in the case of InP and CdSe, it was demonstrated that the number of QDs[39,41] and the final QD diameter[40] can be tuned by the precursor concentrations. In addition to these studies, recent work on the kinetics of the hot injection synthesis showed that the actual solute or monomer is formed *in situ* in the reaction mixture out of the injected precursors.[42,43] Although this has been taken into account in rate equation based models for the formation of colloidal nanocrystals,[44] there is as yet no link between these models and the above-mentioned strategies for size control. This hampers the development of high-yield syntheses, which is an important limiting factor for large-scale applications of colloidal nanocrystals.

In this work, we use a comprehensive model of nucleation and growth that combines classical nucleation theory with the concept of monomer formation to demonstrate that the formation rate of the solute can be used to control d_{PF}. Experimentally verifiable fingerprints of this model synthesis are a three-stage development of the size dispersion from defocusing to focusing to defocusing, where the minimum in the size dispersion is reached close to full yield, and a reaction yield development that is determined by the rate of solute or monomer formation. We show that the time development of a CdSe synthesis, which is optimized for small sizes,[45] is fully in line with the basic features of this model synthesis. On the basis of this correspondence, we explore the tuning of the postfocused size by the reaction rate by varying the precursor concentrations and the reaction temperature. We find that the postfocused size can be adjusted as predicted by the modeling and show that the same approach applies to the synthesis of CdS QDs. This demonstrates that the reaction rate is a powerful reaction variable to steer the outcome of a hot injection synthesis at full yield and narrow size dispersion.

RESULTS

Overview of the Hot Injection Model Synthesis. To understand the development of a colloidal nanocrystal synthesis, it was usually assumed that the injected precursors are the actual solutes.[27] As a result, theoretical descriptions often used a static view of the solute concentration. More recently, Steckel *et al.*[42] and Liu *et al.*[43] demonstrated that formation of the solute from the precursors precedes the precipitation reaction. In line with these results, the hot injection model synthesis developed here assumes a two-step reaction where the injected precursors P first react to form the solute or monomer M, which leads to the nucleation and growth of nanocrystals or QDs in a second stage:

$$\mathrm{P} \rightarrow \mathrm{M} \rightleftharpoons \mathrm{QD} \qquad (1)$$

This makes the time-dependent concentrations of precursors, monomers, and QDs the central quantities of the simulation. These are obtained here by applying the expressions of classical nucleation theory to the monomers (see Supporting Information S1), in line with the approach introduced in general terms by Sugimoto[46] and applied by Kwon *et al.*[47] to the heating-up synthesis of iron oxide nanocrystals. This means that the critical radius, r_c, and the nucleation rate, J_N, are defined in terms of a supersaturation, S, which is defined as the ratio of the monomer concentration and the monomer solubility (γ: QD surface tension, v_0: molecular volume of the QD material, k_B: Boltzmann's constant, D: monomer diffusion coefficient, T: temperature):

$$r_c = \frac{2\gamma v_0}{k_B T \ln S} \qquad (2)$$

$$J_N = \frac{2D}{v_0^{5/3}} \exp\left(-\frac{16\pi\gamma^3 {v_0}^2}{3(k_B T)^3 (\ln S)^2} \right) \qquad (3)$$

Figure 1 represents the outcome of a typical model synthesis, representative of a fast reaction with a low monomer solubility (see Supporting Information S2). Apart from the nucleation stage, the time evolution of the concentration distribution $c(r,t)$ (Figure 1a) resembles the result obtained by Rempel *et al.*,[44] who kept track of all possible n-clusters in the system. Looking at the development of the QD concentration, [QD] (Figure 1b), one sees that there are two main regions in the reaction development: a first in which [QD] increases because of nucleation of new QDs (region 1) and a second where [QD] decreases due to Ostwald ripening (regions 2a and 2b).

In the initial stage of the nucleation (region 1), the generated monomers are mainly consumed by the nucleation of QDs (Figure 1d). Importantly, this implies that the initial nucleation rate and therefore S and r_c are set by the rate of the monomer formation. As a result, [QD] increases with time and the initial size distribution is narrow and centered around a fixed radius. With the rise of [QD], an increasing part of the generated monomers is used for the growth of existing QDs at the expense of nucleation. The dropping nucleation rate

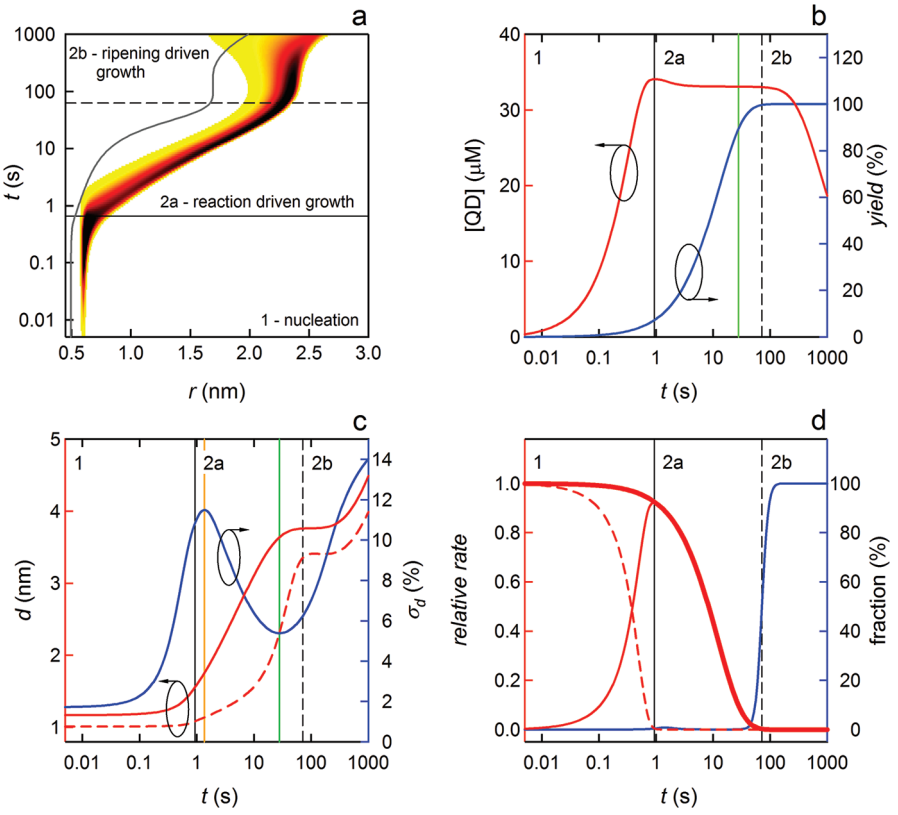

Figure 1. (a) Concentration distribution $c(r,t)$ obtained with the initial parameters as given in the Supporting Information. The color scale indicates an increase of c in the direction yellow−orange−red−black. The gray line marks the critical radius, r_c. (b) Change of (red) QD concentration and (blue) reaction yield as a function of time. (c) Change of (full red) QD diameter, (dashed red) critical radius, and (blue) size dispersion as a function of time. Indicated are (orange) the maximum and (green) the minimum of the size dispersion. (d) (bold red line) Monomer generation rate, (dashed red line) monomer consumption rate by nucleation, and (red line) monomer consumption rate by growth. All rates are given relative to the initial monomer formation rate. (blue) Fraction of the monomer generation resulting from particle dissolution.

results in a reduction of S, and thus an increase of r_c (Figure 1c). When r_c falls within the concentration distribution (Figure 1a), particles with a radius r_{QD} below r_c will dissolve (Ostwald ripening). This results in a maximum [QD], determined by a balance between the dissolution of existing QDs and the nucleation of new QDs. This indicates that Ostwald ripening may occur in parallel with nucleation and is not limited to the end of the reaction, when the monomer concentration is depleted.[28] Opposite of Kwon *et al.*,[47] we find no bimodal concentration distribution in the nucleation region. Since for radii close to r_c, the QD growth rate dr_{QD}/dt increases with r_{QD} (see Supporting Information S1),[48] the onset of QD growth leads to a strong increase of the size dispersion, σ_d, defined here as the ratio between standard deviation of the particle size distribution and r_{QD} (defocusing, Figure 1c).

After the concentration maximum, the contribution of nucleation to the consumption of monomers becomes negligible and the reaction enters a regime in which the monomer generation mainly drives nanocrystal growth (region 2a). This results in a pronounced increase of r_{QD} and a reduction of σ_d (focusing, between orange and green lines in Figure 1c), which is linked to an increasing difference between r_{QD} and r_c (Figure 1c). Opposite of the original description of size distribution focusing,[28] Ostwald ripening is not absent during focusing, but its effect is small and [QD] is almost constant. With increasing reaction time, the monomer generation rate drops, which results in a reduction of the QD growth rate and a progressive decrease of S. Therefore, the difference between r_{QD} and r_c goes down again (Figure 1c) and Ostwald ripening becomes the dominant growth process (region 2b). Hence, σ_d reaches a minimum and further QD growth occurs only at the expense of defocusing and a drop in [QD] (Figure 1b,c). Importantly, the minimum of σ_d corresponds to a reaction yield of 90%. In view of size control at almost full yield, this is an ideal point to stop the reaction, especially since the transition from reaction-driven growth to Ostwald ripening shows a relatively wide time span in which the reaction has reached almost full yield, r_{QD} rises slowly, and σ_d is close to its minimum. This shows the relevance of strategies to tune the diameter at the end of the focusing, i.e., the postfocused diameter d_{PF}.

The connection between size distribution focusing and the difference between r_{QD} and r_c that follows

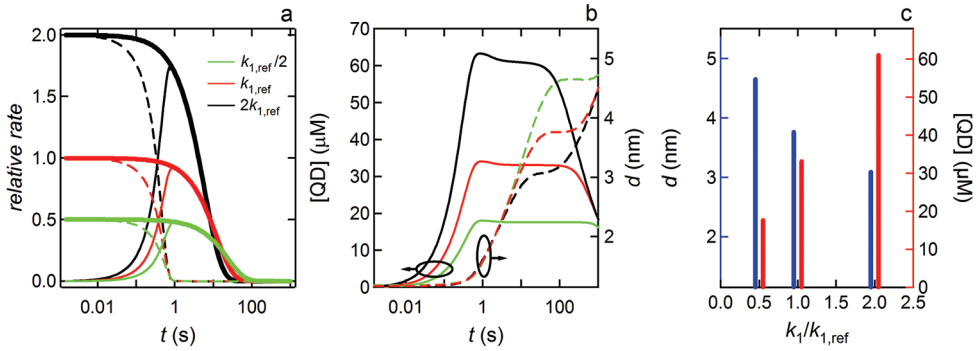

Figure 2. (a) (bold lines) Monomer generation rate; (full lines) rate of monomer consumption by growth; (dashed lines) rate of monomer consumption by nucleation for three different values of the first-order rate constant of monomer generation. Red: the value used in Figure 1 (k_1). Green: $k_1/2$. Black: $2k_1$. (b) (full lines) Change of the QD concentration and (dashed lines) the average QD diameter as a function of time. (c) (blue bars) QD diameter and (red bars) QD concentration at the end of the focusing regime.

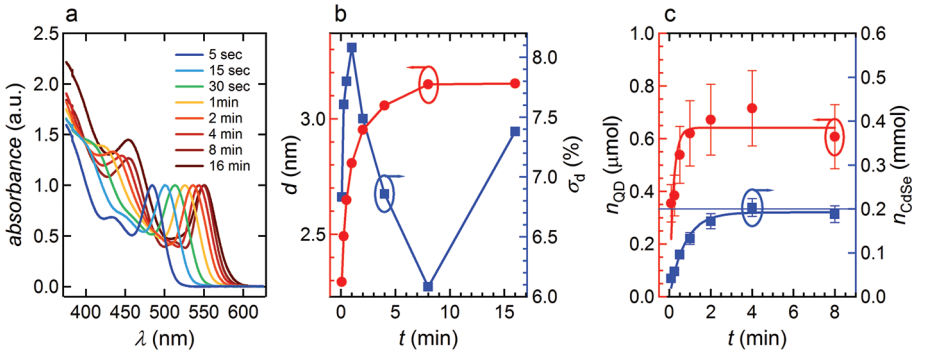

Figure 3. (a) Development of the absorption spectrum of CdSe QDs during a standard synthesis ($n_{Cd,0}$ = 0.2 mmol, $n_{Se,0}$ = 2 mmol, 245 °C/230 °C injection/growth temperature). (b) Time development of (red circles) the QD diameter d and (blue squares) the size dispersion. (c) Time development of the number of QDs (n_{QD}, red circles) and the amount of CdSe formed (n_{CdSe}, blue squares). The full lines are guides to the eye. The horizontal blue line indicates the 100% yield level.

from the modeling (Figure 1c) has been proposed before by Sugimoto[46] and was the subject of a recent theoretical study on focusing during nanocrystal growth by Clark *et al.*[49] Briefly, these authors argue that focusing will occur when r_{QD}/r_c exceeds 2. As shown in the Supporting Information (S4), also in the model synthesis proposed here, the ratio r_{QD}/r_c is a good indicator of focusing. However, the critical value of 2 is not retrieved, possibly due to the different expression for the growth rate used here.[48]

Controling the Postfocused Diameter by the Monomer Formation Rate. Figure 1d represents the three terms contributing to the change of the monomer concentration: monomer generation (G_M, bold line) and monomer consumption by growth (J_G, full line) and by nucleation (J_N, dashed line). One sees that for the fast reaction modeled here, the sum of J_N and J_G is always equal to G_M. Returning to the model, this implies that the supersaturation S is quasi-stationary; that is, dS/dt is small with respect to these three rates. Therefore, the initial nucleation rate is set by the initial monomer generation rate. This implies that the latter may be used to adjust the total number of particles nucleated and, therefore, d_{PF}.

Figure 2a shows G_M, J_N, and J_G for different monomer generation rates (*i.e.*, different first-order rate constants k_1 for the monomer generation reaction). As expected, G_M drops faster for higher reaction rates and the initial nucleation rate changes proportionally to k_1. However, changing k_1 has only a minor effect on the moment that Ostwald ripening exceeds nucleation. This results from the extreme dependence of the nucleation rate on S (see Supporting Information S1), which implies that a change of G_M hardly affects the initial supersaturation and, thus, the initial r_c. Therefore, not only J_N but also the number of particles formed by nucleation is proportional to G_M. This implies that also monomer consumption by growth scales proportionally to G_M and, thus, that the takeover of nucleation by growth hardly changes. The net effect is an increase of the QD concentration during the reaction-driven growth regime with increasing k_1 (Figure 2b). As the total amount of precursor stays constant, this implies that d_{PF} decreases if k_1 is raised. Since a 4-fold increase of k_1 leads to a significant reduction of d_{PF} in the model synthesis, this clearly is a potentially powerful tuning strategy.

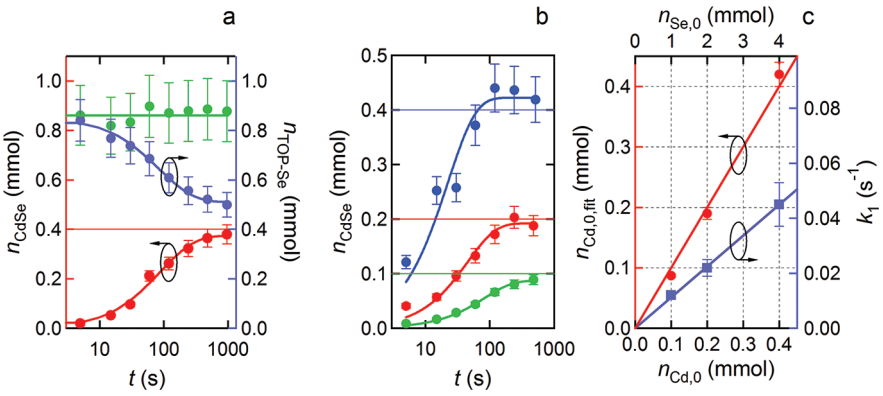

Figure 4. (a) Time evolution of the amount of (red) CdSe (n_{CdSe}), (blue) TOP-Se ($n_{TOP\text{-}Se}$), and (green) the sum of both ($n_{Cd,0}$, 0.4 mmol; $n_{Se,0}$, 1 mmol, 245 °C/230 °C injection/growth temperature). The red and blue fitting lines are guides to the eye, whereas the green line indicates the number of moles of TOP-Se effectively injected (0.86 mmol). The horizontal red line shows the 100% yield level. (b) Time evolution of the amount of CdSe (n_{CdSe}) for reactions with a $n_{Cd,0}$:$n_{Se,0}$ ratio of 1:10, $n_{Cd,0}$ ranges from (green) 0.1 mmol to (red) 0.2 mmol to (blue) 0.4 mmol, 245 °C/230 °C injection/growth temperature. The full lines through the data points represent best fits to eq 4. The horizontal lines indicate the respective 100% yield levels. (c) Fitting parameters, (red) $n_{Cd,0}$ and (blue) k_1, obtained from a best fit of the data shown in (b) to a first-order buildup curve.

Overview of the CdSe Synthesis Used. To verify the predictions of the simulations, we use a synthesis for zincblende CdSe QDs, based on the injection of trioctylphosphine selenide (TOP-Se) in a solution of Cd stearate ($Cd(StA)_2$), hexadecylamine (HDA), and stearic acid (StA) in octadecene (ODE).[45] The typical development of the absorption spectra during the synthesis is shown in Figure 3a. A relatively sharp absorption peak corresponding to the first exciton transition ($\lambda_{1S\text{-}1S}$) is observed even in the beginning of the reaction. With increasing reaction time, $\lambda_{1S\text{-}1S}$ shifts to longer wavelengths, reflecting QD growth. Figure 3b gives the corresponding change of d_{QD} and σ_d with time. In line with the model synthesis, the growth almost stops after σ_d has reached its minimum. Further, a pronounced increase of n_{QD} is observed in the beginning, accompanied by an increase of σ_d. When this defocusing turns into focusing, n_{QD} remains largely constant within the errors of the measurement, in line with the reaction-driven growth regime that appeared in the model synthesis. Moreover, at the end of the focusing regime, the reaction has reached almost full yield. With such a high yield at the postfocused diameter and the almost perfect agreement with the model synthesis, this particular reaction is well suited to investigate the modeling results in terms of tuning d_{PF} by the reaction rate.

CdSe Formation Rate. A key element of the modeling work is that a change of the monomer formation rate enables a tuning of d_{PF}. Hence to implement and understand this tuning strategy, the kinetics of the monomer formation reaction must be known. In the model synthesis, the rate at which CdSe is formed (the CdSe formation rate) equals the rate of monomer generation. To verify this for the experimental synthesis, Figure 4a plots the amount of TOP-Se ($n_{TOP\text{-}Se}$)—as determined using ^{31}P NMR—and CdSe (n_{CdSe}) in the reaction mixture as a function of time. Since the sum of both is a constant, the disappearance of TOP-Se is balanced by the formation of CdSe. This means that the monomer concentration is quasi-stationary, in line with the model synthesis, and that the time development of n_{CdSe} reflects the kinetics of the monomer generation in the experimental synthesis. Figure 4b shows n_{CdSe} as a function of time for three different combinations of $n_{Cd,0}$ and $n_{Se,0}$ under conditions of a 10-fold excess of Se. The thin horizontal lines indicate the 100% yield level for the different reactions (Cd-based), confirming that the Cd precursor is almost completely converted into CdSe for all three reactions. The full lines represent best fits of the experimental data to a model where the formation of CdSe depends in first order on n_{Cd} (see Supporting Information S5):

$$n_{CdSe}(t) = n_{Cd,0}(1 - e^{-k_1 t}) \quad (4)$$

The correspondence between this simple buildup model and the experimental data is surprisingly good.

A closer look at the fitting parameters represented in Figure 4c shows that the fitted value of $n_{Cd,0}$ almost corresponds to the experimental one, as expected for a yield close to 100%. More importantly, we find that the rate constant k_1 increases proportionally to the precursor concentration. Since the ratio $n_{Cd,0}$:$n_{Se,0}$ was kept constant during these experiments, this suggests that the formation of CdSe is determined by a second-order monomer generation rate, which is proportional either to n_{Cd}^2 or to $n_{Cd} \times n_{Se}$.

To investigate this more closely, the development of n_{CdSe} with time was determined at two different temperatures and for various combinations of $n_{Cd,0}$ and $n_{Se,0}$ (Figure 5a and b). For these experiments, the concentration of StA and HDA was adjusted proportionally to $n_{Cd,0}$. As demonstrated in the Supporting Information (S6), the reaction rate does not depend on the concentration of StA or HDA. Thus, differences in

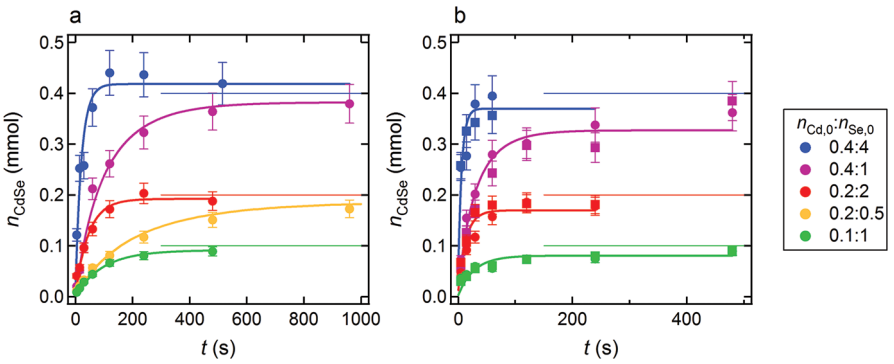

Figure 5. (a) Time evolution of the amount of CdSe formed (n_{CdSe}) for reactions with initial amounts $n_{Cd,0}$ and $n_{Se,0}$ as indicated in the legend (all numbers in mmol), 245 °C/230 °C injection/growth temperature. The horizontal lines indicate the respective 100% yield levels. The full lines through the data points represent best fits using a monomer generation rate that is first order in P_{Cd} and P_{Se}. (b) The same as in (a) using 280 °C/260 °C as injection/growth temperature. Note the different scale in the horizontal axis. The squares and the circles indicate different runs of the same experiment.

the yield development between different experiments directly reflect the influence of the precursor concentration on the reaction rate. Figure 5a and b show that reactions where the product $n_{Cd,0} \times n_{Se,0}$ is the same (purple and red data, orange and green data) have a coinciding slope dn_{CdSe}/dt at $t = 0$ and, thus, an identical initial reaction rate. Furthermore, for reactions with the same $n_{Cd,0}$, the initial rate dn_{CdSe}/dt increases proportionally to $n_{Se,0}$ (see Figure 5a, b and Supporting Information S5). Both elements point toward a rate equation that depends in first order on n_{Cd} and n_{Se}.

To corroborate this conclusion, we have fitted the experimental development of $n_{CdSe}(t)$ to a buildup curve based on a formation rate that is proportional to $n_{Cd,0} \times n_{Se,0}$ (see Supporting Information S5). In these fits, a single value is used for the second-order rate constant k_2 and $n_{Cd,0}$ is taken as an adjustable variable to compensate for reaction yields slightly different from 100%. As shown in Figure 5a and b, the agreement between the data and the best fit is remarkable and results in second-order rate constants of 0.14 ± 0.01 L/(s mol) at 230 °C and 0.56 ± 0.05 L/(s mol) at 260 °C. The fact that the formation of CdSe with time follows this simple second-order rate law, which is independent of the QD size and concentration, confirms that the CdSe formation is dominated by a monomer generation in solution and barely by a surface reaction of the separate precursors. Moreover, the first-order dependence of the CdSe formation rate on n_{Cd} and n_{Se} excludes the possibility that the monomers are in quasi-equilibrium with the precursors. Indeed, if this would be true, the rate of CdSe formation can be proportional to $n_{Cd,0} \times n_{Se,0}$ only if the rate of monomer consumption by nucleation and growth depends in first order on the monomer concentration, which is not the case (see eq 3 and Supporting Information S1) .

Steckel *et al.* and Liu *et al.*[42,43] proposed a possible mechanism for the monomer formation in reactions similar to the one used here, involving the formation of a cadmium selenide complex (binding reaction), which decomposes further to a CdSe monomer (cleavage reaction):

$$Cd(OOCR)_2 + SePR_3 \underset{k_{-b}}{\overset{k_b}{\rightleftharpoons}} [Cd(OOCR)(SePR_3)]^+[OOCR]^- \quad (5)$$

$$[Cd(OOCR)(SePR_3)]^+[OOCR]^- \xrightarrow{k_c} CdSe + OPR_3 + O(OCR)_2 \quad (6)$$

In line with this mechanism, we find that the disappearance of TOP-Se results in the formation of an equivalent amount of TOPO (see Supporting Information S7). Hence, assuming that the above reaction scheme applies, the experimentally observed second-order rate equation indicates that the concentration of the complex is quasi-stationary, which leads to an effective second-order rate constant, $k_{2,eff} = k_c k_b/(k_c + k_{-b})$. In the limit $k_c \gg k_{-b}$, this implies that the binding reaction is rate determining, while if $k_c \ll k_{-b}$, the binding reaction (5) is in rapid, quasi-equilibrium and the cleavage reaction is rate determining. A similar result was found by Owen *et al.* for cadmium phosphonate/TOPSe-based hot injection reactions.[39] However, the fact that the CdSe formation rate does not depend on the concentration of added carboxylic acid or alkyl amines (see Supporting Information)—which are both nucleophiles that can enhance the cleavage reaction—suggests that in this case the binding reaction is rate limiting.

With the monomer formation rate depending in first order on both precursors, the particular CdSe synthesis used here represents an ideal system for investigating the tuning of d_{PF} by the reaction rate. In the case of a Se excess for example, the pseudo-first-order rate constant of the monomer formation reaction is proportional to $n_{Se,0}$ (Figure 4). Therefore, changing $n_{Se,0}$ suffices to analyze the predicted link between the monomer formation rate and d_{PF}.

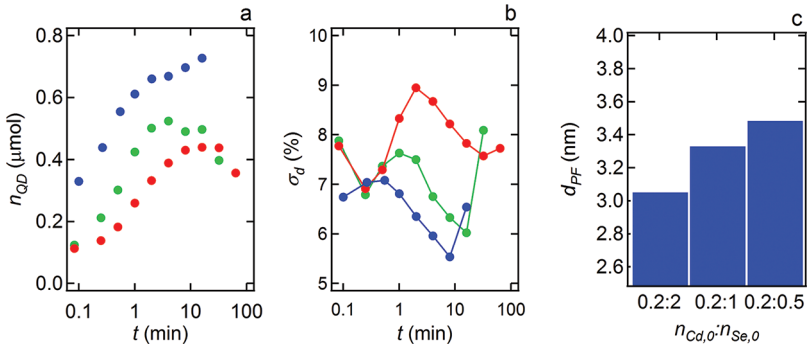

Figure 6. (a) Time evolution of the amount of QDs for reactions with $n_{Cd,0}$:$n_{Se,0}$ of (blue) 0.2:2, (green) 0.2:1, and (red) 0.2:0.5 (numbers in mmol), 245 °C/230 °C injection/growth temperature. (b) Time evolution of the size dispersion for the same reactions as in (a). (c) Postfocused diameter of the different reactions.

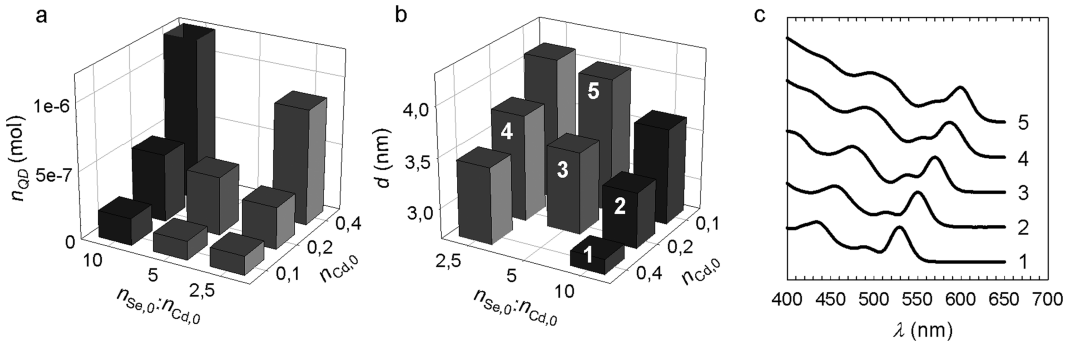

Figure 7. (a) Concentration of QDs formed as a function of $n_{Cd,0}$ and the $n_{Se,0}$:$n_{Cd,0}$ ratio; 280 °C/260 °C injection/growth temperature. (b) Postfocused diameter obtained as a function of $n_{Cd,0}$ and the $n_{Se,0}$:$n_{Cd,0}$ ratio. Note that the direction of each axis is swapped with respect to (a). (c) Absorption spectrum corresponding to the samples as indicated in (b).

Tuning d_{PF} by the Reaction Rate: Role of the Precursor Concentration. Figure 6 shows the development of n_{QD} and σ_d for three reactions with constant $n_{Cd,0}$, while $n_{Se,0}$:$n_{Cd,0}$ is increased from 2.5 to 5 to 10. All reactions follow the general behavior of the model synthesis, with σ_d reaching its minimum at almost full yield. Moreover, in line with the model predictions (Figure 2), n_{QD} goes down when $n_{Se,0}$ is decreased, and a larger d_{PF} is hence obtained for lower reaction rates (Figure 6c). Obviously, the time at which d_{PF} is reached increases when the reaction rate is reduced (Figure 6b).

As shown in Figure 7 and Table 1, this result can be generalized to different initial precursor concentrations. Doubling $n_{Cd,0}$ and $n_{Se,0}$ roughly leads to a 3-fold increase of the number of QDs. As expected from the CdSe formation kinetics, a separate increase of the cadmium, or the selenium precursor, leads to an increase of the number of nuclei as well, which is more pronounced when increasing the cadmium concentration. However, since the selenium precursor was kept in excess during this study, the absolute reaction yield goes up as well when the cadmium precursor concentration is increased. This makes size control by adjusting the selenium precursor concentration more efficient. Overall, changing the product $n_{Cd,0} \times n_{Se,0}$ by a factor of 64 allows us to vary the QD diameter from 2.8 to 4.1 nm and the position of the first electronic transition ($\lambda_{1S\text{-}1S}$) from 529 to 601 nm with reaction yields in the range of 90% and low size dispersions (Figure 7, Table 1). Hence, this approach represents a simple yet powerful strategy to tune d_{PF} in a hot injection

TABLE 1. Summary of the Reaction Time, Wavelength of the First Exciton Transition, Postfocused Diameter, and Number of QDs Formed for Different Combinations of $n_{Cd,0}$ and the $n_{Se,0}$:$n_{Cd,0}$ Ratio at 280 °C/260 °C Injection/Growth Temperature[a]

		$n_{Cd,0}$ (mmol)		
$n_{Se,0}$:$n_{Cd,0}$		0.4	0.2	0.1
10:1	time (min)	1	2	8
	$\lambda_{1S\text{-}1S}$ (nm)	528.8 ± 2.9	550.9 ± 0.2	579.5 ± 3.8
	d (nm)	2.85 ± 0.04	3.19 ± 0.05	3.65 ± 0.07
	n_{QD} (10^{-6} mol)	1.33 ± 0.05	0.56 ± 0.1	0.20 ± 0.01
5:1	time (min)		8	32
	$\lambda_{1S\text{-}1S}$ (nm)		571.7 ± 3.4	598.2 ± 0.6
	d (nm)		3.51 ± 0.06	4.02 ± 0.01
	n_{QD} (10^{-6} mol)		0.43 ± 0.02	0.14 ± 0.01
2.5:1	time (min)	8	32	128
	$\lambda_{1S\text{-}1S}$ (nm)	569.2 ± 0.5	585 ± 1.1	601.4 ± 0.2
	d (nm)	3.46 ± 0.01	3.75 ± 0.02	4.10 ± 0.01
	n_{QD} (10^{-6} mol)	0.86 ± 0.04	0.31 ± 0.02	0.14 ± 0.010

[a] For all reactions, the yield amounts to 85–95%.

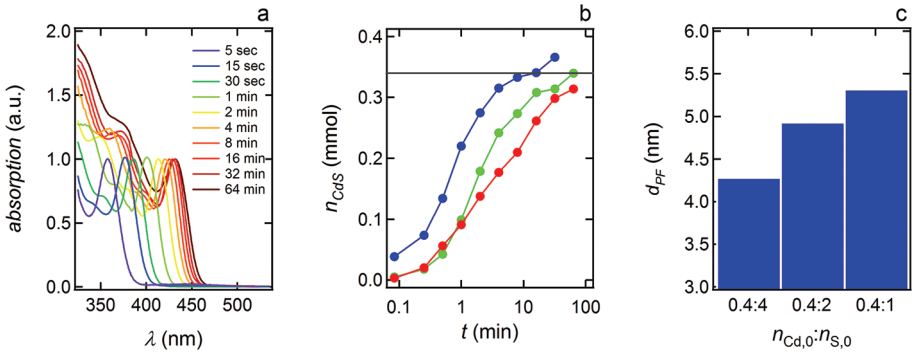

Figure 8. Size tuning in the CdS synthesis, showing (a) the evolution of the absorption spectra as a function of time ($n_{Cd,0}$ = 0.4 mmol, $n_{S,0}$ = 4 mmol). (b) Evolution of the amount of CdS formed as a function of time for reactions with $n_{Cd,0}$:$n_{S,0}$ of (blue) 0.4:4, (green) 0.4:2, and (red) 0.4:1 (numbers in mmol). The horizontal line shows the 85% yield level. (c) Postfocused diameter of the different reactions. For all reactions, 280 °C/260 °C was used as injection/growth temperature, respectively.

synthesis, albeit at the expense of an increased reaction time and a reduction of the amount of material produced for larger sizes.

In the simulations, reducing k_1 by a factor of 4 increases d_{PF} by about 50% from 3.0 to 4.6 nm. Experimentally, a more moderate increase from 2.8 to 4.1 nm is achieved by changing $n_{Se,0}$ and $n_{Cd,0}$ over a range that approximately corresponds to a 16-fold increase of the pseudo-first-order rate constant. This more limited tuning in the experimental system can be linked to the duration of the nucleation. Opposite of the simulations, Figure 6a and b indicate that the rise of n_{QD} and the initial defocusing last longer if the monomer generation rate is reduced. For example, the moment the maximum in the size dispersion is reached increases from 15 s up to 1 min when $n_{Se,0}$ is reduced from 2 to 0.5 mmol. This prolonged nucleation implies that a reduction of the monomer formation rate reduces n_{QD} less than predicted by the modeling, which leads in turn to a smaller than expected increase of d_{PF}. Within the logic of the simulations, the experimentally observed prolonged nucleation indicates that the dependence of the nucleation rate on S is less extreme than expressed by eq 3, an expression typically used to describe the nucleation event in a hot injection synthesis.[27,47,50] According to classical nucleation theory, the nucleation rate is linked to the free energy barrier $\Delta_N G$ for nucleation:

$$\Delta_N G = \frac{16\pi\gamma^3 v_0^2}{3(k_B T)^2 (\ln S)^2} = \frac{4\pi}{3}\gamma r_c^2 \qquad (7)$$

Hence, the experimentally observed persistence of the nucleation at larger r_c (or lower supersaturation) implies that $\Delta_N G$ increases less strongly than assumed with increasing r_c. Following eq 7, this could for example result from a reduction of the surface tension with increasing QD diameter, which is not unexpected given the strong reduction of the surface curvature that accompanies QD growth. The occurrence of a

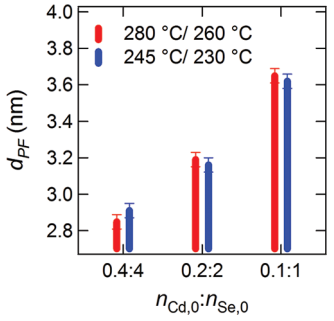

Figure 9. Postfocused diameter obtained for different initial concentrations at two different combinations of injection and growth temperature.

prolonged nucleation also indicates that hot injection followed by burst nucleation is not required to obtain narrow size distributions, opposite of what is often proposed in the description of the hot injection synthesis.[27]

Size Tuning in the CdS Synthesis. Since the model synthesis is not material specific, the proposed tuning strategy should not be limited to a particular CdSe synthesis. To demonstrate this, Figure 8 represents a study on CdS QDs, where we again explore size tuning by changing the initial precursor concentrations. As shown in Figure 8a, the absorption peak corresponding to the first exciton transition can be used to determine the average particle diameter. Regardless of the precursor concentration, the synthesis runs to almost full yield—the black line in Figure 8b indicates the 85% yield level—and we find again that lowering the concentration of the S precursor slows the CdS formation. In line with the model synthesis, a reduction of the CdS formation rate leads to an increase of the nanocrystal diameter (Figure 8c). This result indicates that adjusting the postfocused size of colloidal nanocrystals by the reaction rate could be a general strategy to obtain colloidal nanocrystals with a predefined diameter and a narrow size dispersion at close to full yield. This conclusion is further supported by the results on wurtzite

CdSe presented by Owen *et al.*,[39] who demonstrate that an increase of the amount of TOP-Se injected raises the QD concentration.

Tuning d_{PF} by the Reaction Rate: Role of Temperature. A classical description of the hot injection synthesis is that the rapid injection of precursors into a hot (surfactant) solution produces a high degree of supersaturation, resulting in a burst nucleation by relieving the excess free energy of the supersaturation.[27] Looking at the expression for the critical radius and the nucleation rate, this should result in the formation of more and smaller nuclei at higher temperature and, thus, a decrease of d_{PF}. A similar conclusion could follow from the viewpoint that the nucleation rate is set by the monomer generation rate, since the second-order rate constant of this reaction increases with temperature. Opposite of this expected trend, Figure 9 shows that the reaction temperature has no significant effect on d_{PF} and thus on the QD concentration. Similarly, Joo *et al.* observed that in the case of the PbSe synthesis, increasing the injection temperature leads to a decrease of the QD concentration during growth and an increase of the QD diameter.[50] These contradictions are hard to reconcile with the classical description linking hot injection to burst nucleation. On the other hand, they can be understood by considering that, next to the monomer formation rate, also the rate of QD nucleation and growth depend on temperature. For example, if an increase of the temperature significantly enhances the growth rate, *e.g.*, linked to an increase of the monomer solubility, the time span of nucleation will be reduced. Since the total number of particles formed during the nucleation stage depends on both the nucleation rate and the time span of nucleation, the net effect of a temperature change on the final QD concentration and diameter is difficult to predict. For the present synthesis, it appears that the net effect of the change of nucleation rate and nucleation time span is that d_{PF} is almost insensitive to a change in temperature. Importantly, this lack of temperature dependence explains the high reproducibility of the postfocused diameter for given conditions as shown in Table 1. Clearly, this is an important advantage of the reaction presented here.

CONCLUSION

This work discusses the tuning of the QD diameter at which the size dispersion is lowest during synthesis, defined as the postfocused diameter, d_{PF}, by the reaction rate. The study combines a simulation of the hot injection synthesis by a rate equation model, which provides the time development of the number of nuclei, the mean particle size, and the size distribution, with an experimental study mainly based on a particular synthesis for CdSe QDs. Both simulation and experiment differ markedly from the traditional hot injection/burst nucleation description. We find that the rate of nucleation is controlled by the rate of *in situ* monomer or solute formation, while its time span depends on the takeover of nucleation by Ostwald ripening. In addition, the change of the critical radius with respect to the mean QD radius leads to a characteristic defocusing−focusing−defocusing development of the size distribution. The insight in the factors controlling nucleation provides a straightforward strategy for tuning d_{PF} by the rate of the monomer formation reaction. After showing that the CdSe formation rate depends in first order on the Cd and the Se precursor, we explore this strategy by adjusting the precursor concentrations. In line with the simulations, we find that an increase of the monomer formation rate leads to a decrease of d_{PF} and *vice versa*. Similar results are obtained with a synthesis of CdS QDs, indicating that the proposed strategy is not limited to a particular QD synthesis and may be more generally applicable. On the other hand, a change of the injection and growth temperatures has little effect on d_{PF}. This indicates that obtaining narrow size distributions by arresting nucleation using a specific temperature program is not required nor possible, since a change of the temperature also directly influences the growth rate. This enhanced understanding supported by a combination of simulations and experiments provides a conceptual basis for developing alternative tuning strategies for the hot injection synthesis. Since this postfocused diameter, d_{PF}, is reached at almost full yield, this is a highly relevant issue with respect to upscaling and automation of the hot injection synthesis.

METHODS

Numerical Modeling. Modeling of the QD synthesis was done by implementing the equations outlined below directly into COMSOL Multiphysics, a commercially available finite-element partial differential equation solver. The parameters used for all simulations are given in the Supporting Information.

Chemicals. Methanol and 2-propanol were purchased from VWR BDH Prolabo and were Rectapur grade. Toluene was also purchased from VWR BDH Prolabo and was technical (for workup) and Normapur grade (for spectroscopy). Oleic acid (90%) and cadmium oxide (CdO; 99.99+%) were purchased from Aldrich. Selenium (99.999%) and 1-octadecene (ODE; tech.) were purchased from Alfa Aesar. Stearic acid (98%) and hexadecylamine (HDA, 90%) were purchased from Merck. Trioctylphospine (TOP, 97%) and sulfur (99.999%) were purchased from Strem. Oleylamine (OLA; approximate C18-content 80−90%) was purchased from Acros Organics.

Precursor Preparation. Cadmium stearate (cadmium to stearic acid ratio 1:3) was prepared by mixing CdO and stearic acid in a 1:3 molar ratio, degassing for 1 h at 100 °C under a nitrogen flow, and dissolving the cadmium oxide under a nitrogen atmosphere between 250 and 300 °C until the mixture became clear.

Cadmium oleate (cadmium to oleic acid ratio 1:3) was prepared with a similar procedure starting from CdO and oleic acid. TOP-Se solutions (solutions of trioctylphosphine selenide in TOP) were prepared by dissolution of elemental selenium in TOP at room temperature under a nitrogen atmosphere. TOP-S solutions (solutions of trioctylphosphine sulfide in TOP) were similarly prepared by dissolution of elemental sulfur in TOP at 110 °C under a nitrogen atmosphere.

Synthesis of CdSe QDs. CdSe QDs were synthesized similar to a recently published procedure:[45] a mixture of cadmium stearate, stearic acid, and HDA (molar ratio 1:2:8) was filled up to a total volume of 10 mL at room temperature in a 25 mL three-neck flask. The reaction mixture was degassed for 30−60 min at room temperature and 60 min at 100 °C under a nitrogen flow. Still under nitrogen, the temperature was raised to the injection temperature (280 or 245 °C), 2 mL of a solution of TOP-Se was injected, and the reaction was performed at a growth temperature of 260 or 230 °C, respectively. Care was taken to avoid any degradation of the Cd precursor in the reaction mixture prior to TOP-Se injection.[40] Aliquots were taken after particular reaction times, dissolved in a 1:5 mixture of oleic acid and toluene, and precipitated with methanol or a 1:1 mixture of methanol and 2-propanol. The precipitate was redissolved in toluene, precipitated a second time with methanol, and again redissolved in toluene. In the article, reactions are characterized by the initial amount of Cd and Se precursor used in mmol, indicated as $n_{Cd,0}$ and $n_{Se,0}$, respectively. Precursor concentrations in mol/L can be obtained by multiplying these numbers with a reference concentration, $c_0 = 1/V$, with V the volume of the reaction mixture in mL. Neglecting the volume change with temperature, c_0 was taken as 1/12 mol/L for the calculation of reaction rate constants. The structural characterization of the resulting QDs, including X-ray powder diffraction and transmission electron microscopy, has been presented before.[51]

Synthesis of CdS Quantum Dots. For the synthesis of CdS QDs we used a procedure similar to the CdSe QD synthesis: a mixture of cadmium stearate, stearic acid, and HDA (molar ratio 1:2:8) was filled up to a total volume of 10 mL at room temperature in a 25 mL three-neck flask. After degassing the reaction mixture for half an hour at room temperature and one hour at 100 °C under a nitrogen flow, the temperature was raised to the injection temperature (280 °C). Then 2 mL of a solution of TOP-S was injected, and the reaction was performed at a growth temperature of 260 °C. The whole synthesis was performed under N_2, and care was taken to avoid any degradation of the Cd precursor in the reaction mixture prior to TOP-S injection. Aliquots were taken and purified in the same manner as during the CdSe QD synthesis. In the article, reactions are characterized by the initial amount of Cd and S precursor used in mmol, indicated as $n_{Cd,0}$ and $n_{S,0}$, respectively.

Optical Characterization. UV−vis absorption spectra were recorded with a Perkin-Elmer Lambda 950 spectrometer. Three different investigations were performed. First, the development of the absorption spectra during a reaction was followed until a degradation of the samples was observed. Aliquots were taken after certain times, dissolved in toluene, and investigated by UV−vis spectroscopy without further workup. Second, to determine the yield at the end of the reaction typically three aliquots were taken for the postfocused time, weighted, purified, and quantitatively investigated. Third, for yield development investigations, consecutive aliquots were taken at specific times after the injection until the reaction reached the postfocused size, which were all weighed, purified, and quantitatively analyzed by UV−vis.

Quantitative Data Analysis. The mean QD diameter, d, is calculated from the peak wavelength of the first exciton transition using the zb-CdSe sizing curve.[51] Using the same sizing curve, the size distribution is estimated from the half-width at half-maximum of the absorption peak of the first exciton transition. This procedure probably overestimates the size dispersion, since it assumes that the broadening of the first exciton peak is caused only by a distribution of QD sizes. The amount of CdSe formed is obtained from the average absorbance of a diluted aliquot at 300, 320, and 340 nm,[51] which is directly proportional to the volume fraction of CdSe and, hence, n_{CdSe}. This implies that the major sources of error on n_{CdSe} comes from a possible error on the absorption coefficients and the limited reproducibility of sampling. This error is estimated at 10%. From d and n_{CdSe}, the quantum dot concentration, n_{QD}, is calculated. Hence, contrary to n_{CdSe}, the determination of this latter quantity is sensitive to errors in the sizing curve. For CdS QDs we obtained n_{CdS} from the diameter and the concentration of QDs following the sizing curve and the extinction coefficients published by Yu *et al.*[52]

^{31}P NMR Analysis. We prepared NMR samples by taking aliquots (200−300 μL) during the synthesis and diluting these without further purification with 300 μL of toluene-d_8 under N_2. The CdSe QD synthesis used for NMR measurements differs from the other syntheses in the use of cadmium oleate, oleic acid, and OLA instead of cadmium stearate, stearic acid, and HDA, respectively, while keeping all other chemicals and parameters identical (*e.g.*, the 1:2:8 molar ratio). This made quantitative NMR measurements of the unpurified samples at room temperature possible because no turbidity was present (as would be the case with the standard synthesis using stearic acid and HDA). NMR data were collected using a Bruker DRX 500 spectrometer (^{1}H and ^{13}C frequency of 500.13 and 125.76 MHz, respectively) equipped with a 5 mm TBI probe (maximum Z-gradient strength of 0.535 T m^{-1}) to record ^{31}P NMR spectra at 202.457 MHz. The quantitative ^{31}P spectra were recorded using a 3 s interscan delay, a spectral width of 398.35 ppm, and 87 248 time domain data points. This delay was calculated to allow over 96% recovery of original magnetization when applying 30° ^{31}P pulses. The temperature was set to 298.16 K. ^{31}P resonances were attributed according to previous published ^{31}P measurements on pure TOP, pure TOP-Se, and TOPO in toluene-d_8.[53,54]

Acknowledgment. The authors thank BelSPo (IAP 6.10, photonics@be), EU FP7 (ITN Herodot), and the FWO-Vlaanderen (grant no. G.0794.10) for funding this research. A. Hassinen is acknowledged for his initial work on the CdS synthesis. Prof. J. C. Martins and F. Van den Broeck are acknowledged for executing the ^{31}P NMR measurements.

Supporting Information Available: Derivation of the model equations, the parameter set for the reference simulation, a movie describing the model synthesis, an analysis of the size-focusing coefficient, the integrated second-order rate equation, the results of the ^{31}P NMR analysis and the reaction rate as a function of carboxylic acid and amine concentration. This material is available free of charge *via* the Internet at http://pubs.acs.org.

REFERENCES AND NOTES

1. Brus, L. E. A Simple-Model for the Ionization-Potential, Electron-Affinity, and Aqueous Redox Potentials of Small Semiconductor Crystallites. *J. Chem. Phys.* **1983**, *79*, 5566–5571.
2. Murray, C. B.; Norris, D. J.; Bawendi, M. G. Synthesis and Characterization of Nearly Monodisperse Cde (E = S, Se, Te) Semiconductor Nanocrystallites. *J. Am. Chem. Soc.* **1993**, *115*, 8706–8715.
3. Hines, M. A.; Guyot-Sionnest, P. Synthesis and Characterization of Strongly Luminescing ZnS-Capped CdSe Nanocrystals. *J. Phys. Chem.* **1996**, *100*, 468–471.
4. Dabbousi, B. O.; RodriguezViejo, J.; Mikulec, F. V.; Heine, J. R.; Mattoussi, H.; Ober, R.; Jensen, K. F.; Bawendi, M. G. (CdSe)ZnS Core-Shell Quantum Dots: Synthesis and Characterization of a Size Series of Highly Luminescent Nanocrystallites. *J. Phys. Chem. B* **1997**, *101*, 9463–9475.
5. Peng, X. G.; Manna, L.; Yang, W. D.; Wickham, J.; Scher, E.; Kadavanich, A.; Alivisatos, A. P. Shape Control of CdSe Nanocrystals. *Nature* **2000**, *404*, 59–61.
6. Bailey, R. E.; Nie, S. M. Alloyed Semiconductor Quantum Dots: Tuning the Optical Properties without Changing the Particle Size. *J. Am. Chem. Soc.* **2003**, *125*, 7100–7106.
7. Kim, S.; Fisher, B.; Eisler, H. J.; Bawendi, M. Type-II Quantum Dots: CdTe/CdSe(core/shell) and CdSe/ZinTe(core/shell) Heterostructures. *J. Am. Chem. Soc.* **2003**, *125*, 11466–11467.

8. Talapin, D. V.; Mekis, I.; Gotzinger, S.; Kornowski, A.; Benson, O.; Weller, H. CdSe/CdS/ZnS and CdSe/ZnSe/ZnS Core-Shell-Shell Nanocrystals. *J. Phys. Chem. B* **2004**, *108*, 18826–18831.
9. Li, J. J.; Wang, Y. A.; Guo, W. Z.; Keay, J. C.; Mishima, T. D.; Johnson, M. B.; Peng, X. G. Large-Scale Synthesis of Nearly Monodisperse CdSe/CdS Core/Shell Nanocrystals Using Air-Stable Reagents via Successive Ion Layer Adsorption and Reaction. *J. Am. Chem. Soc.* **2003**, *125*, 12567–12575.
10. Carbone, L.; Nobile, C.; De Giorgi, M.; Sala, F. D.; Morello, G.; Pompa, P.; Hytch, M.; Snoeck, E.; Fiore, A.; Franchini, I. R.; Nadasan, M.; Silvestre, A. F.; Chiodo, L.; Kudera, S.; Cingolani, R.; Krahne, R.; Manna, L. Synthesis and Micrometer-Scale Assembly of Colloidal CdSe/CdS Nanorods Prepared by a Seeded Growth Approach. *Nano Lett.* **2007**, *7*, 2942–2950.
11. Pietryga, J. M.; Werder, D. J.; Williams, D. J.; Casson, J. L.; Schaller, R. D.; Klimov, V. I.; Hollingworth, J. A. Utilizing the Lability of Lead Selenide to Produce Heterostructured Nanocrystals with Bright, Stable Infrared Emission. *J. Am. Chem. Soc.* **2008**, *130*, 4879–4885.
12. Dorfs, D.; Salant, A.; Popov, I.; Banin, U. ZnSe Quantum Dots within CdS Nanorods: A Seeded-Growth Type-II System. *Small* **2008**, *4*, 1319–1323.
13. Garcia-Santamaria, F.; Chen, Y. F.; Vela, J.; Schaller, R. D.; Hollingsworth, J. A.; Klimov, V. I. Suppressed Auger Recombination in "Giant" Nanocrystals Boosts Optical Gain Performance. *Nano Lett.* **2009**, *9*, 3482–3488.
14. Talapin, D. V.; Lee, J.-S.; Kovalenko, M. V.; Shevchenko, E. V. Prospects of Colloidal Nanocrystals for Electronic and Optoelectronic Applications. *Chem. Rev.* **2009**, *110*, 389–458.
15. Srivastava, S.; Kotov, N. A. Composite Layer-by-Layer (LBL) Assembly with Inorganic Nanoparticles and Nanowires. *Acc. Chem. Res.* **2008**, *41*, 1831–1841.
16. Kotov, N. A.; Meldrum, F. C.; Wu, C.; Fendler, J. H. Monoparticulate Layer and Langmuir-Blodgett-Type Multiparticulate Layers of Size-Quantrized Cadmium-Sulfide Clusters—a Colloid-Chemical Approach to Superlattice Construction. *J. Phys. Chem.* **1994**, *98*, 2735–2738.
17. Lambert, K.; Capek, R. K.; Bodnarchuk, M. I.; Kovalenko, M. V.; Van Thourhout, D.; Heiss, W.; Hens, Z. Langmuir—Schaefer Deposition of Quantum Dot Multilayers. *Langmuir* **2010**, *26*, 7732–7736.
18. McDonald, S. A.; Konstantatos, G.; Zhang, S. G.; Cyr, P. W.; Klem, E. J. D.; Levina, L.; Sargent, E. H. Solution-Processed PbS Quantum Dot Infrared Photodetectors and Photovoltaics. *Nat. Mater.* **2005**, *4*, 138–U14.
19. Rauch, T.; Boberl, M.; Tedde, S. F.; Furst, J.; Kovalenko, M. V.; Hesser, G. N.; Lemmer, U.; Heiss, W.; Hayden, O. Near-infrared Imaging with Quantum-Dot-Sensitized Organic Photodiodes. *Nat. Photonics.* **2009**, *3*, 332–336.
20. Coe, S.; Woo, W. K.; Bawendi, M.; Bulovic, V. Electroluminescence from Single Monolayers of Nanocrystals in Molecular Organic Devices. *Nature* **2002**, *420*, 800–803.
21. Caruge, J. M.; Halpert, J. E.; Wood, V.; Bulovic, V.; Bawendi, M. G. Colloidal Quantum-Dot Light-Emitting Diodes with Metal-Oxide Charge Transport Layers. *Nat. Photonics* **2008**, *2*, 247–250.
22. Vogel, R.; Hoyer, P.; Weller, H. Quantum-Sized PbS, CdS, Ag_2S, Sb_2S_3, and Bi_2S_3 Particles as Sensitizers for Various Nanoporous Wide-Bandgap Semiconductors. *J. Phys. Chem.* **1994**, *98*, 3183–3188.
23. Johnston, K. W.; Pattantyus-Abraham, A. G.; Clifford, J. P.; Myrskog, S. H.; MacNeil, D. D.; Levina, L.; Sargent, E. H. Schottky-Quantum Dot Photovoltaics for Efficient Infrared Power Conversion. *Appl. Phys. Lett.* **2008**, *92*, 151115.
24. Luther, J. M.; Law, M.; Beard, M. C.; Song, Q.; Reese, M. O.; Ellingson, R. J.; Nozik, A. J. Schottky Solar Cells Based on Colloidal Nanocrystal Films. *Nano Lett.* **2008**, *8*, 3488–3492.
25. Medintz, I. L.; Uyeda, H. T.; Goldman, E. R.; Mattoussi, H. Quantum Dot Bioconjugates for Imaging, Labelling and Sensing. *Nat. Mater.* **2005**, *4*, 435–446.
26. Somers, R. C.; Bawendi, M. G.; Nocera, D. G. CdSe Nanocrystal Based Chem-/Bio-sensors. *Chem. Soc. Rev.* **2007**, *36*, 579–591.
27. Park, J.; Joo, J.; Kwon, S. G.; Jang, Y.; Hyeon, T. Synthesis of Monodisperse Spherical Nanocrystals. *Angew. Chem., Int. Ed.* **2007**, *46*, 4630–4660.
28. Peng, X. G.; Wickham, J.; Alivisatos, A. P. Kinetics of II-VI and III-V Colloidal Semiconductor Nanocrystal Growth: "Focusing" of Size Distributions. *J. Am. Chem. Soc.* **1998**, *120*, 5343–5344.
29. Talapin, D. V.; Rogach, A. L.; Kornowski, A.; Haase, M.; Weller, H. Highly Luminescent Monodisperse CdSe and CdSe/ZnS Nanocrystals Synthesized in a Hexadecylamine-Trioctylphosphine Oxide-Trioctylphospine Mixture. *Nano Lett.* **2001**, *1*, 207–211.
30. Murray, C. B.; Sun, S. H.; Gaschler, W.; Doyle, H.; Betley, T. A.; Kagan, C. R. Colloidal Synthesis of Nanocrystals and Nanocrystal Superlattices. *IBM J. Res. Dev.* **2001**, *45*, 47–56.
31. Peng, Z. A.; Peng, X. G. Formation of High-Quality CdTe, CdSe, and CdS Nanocrystals Using CdO As Precursor. *J. Am. Chem. Soc.* **2001**, *123*, 183–184.
32. Jasieniak, J.; Bullen, C.; van Embden, J.; Mulvaney, P. Phosphine-free synthesis of CdSe nanocrystals. *J. Phys. Chem. B* **2005**, *109*, 20665–20668.
33. Hines, M. A.; Scholes, G. D. Colloidal PbS Nanocrystals with Size-Tunable Near-Infrared Emission: Observation of Post-synthesis Self-Narrowing of the Particle Size Distribution. *Adv. Mater.* **2003**, *15*, 1844–1849.
34. Xie, R.; Battaglia, D.; Peng, X. Colloidal InP Nanocrystals As Efficient Emitters Covering Blue to Near-Infrared. *J. Am. Chem. Soc.* **2007**, *129*, 15432–+.
35. Li, L.; Daou, T. J.; Texier, I.; Tran, T. K. C.; Nguyen, Q. L.; Reiss, P. Highly Luminescent $CuInS_2$/ZnS Core/Shell Nanocrystals: Cadmium-Free Quantum Dots for In Vivo Imaging. *Chem. Mater.* **2009**, *21*, 2422–2429.
36. Yu, W. W.; Peng, X. G. Formation of high-quality CdS and Other II-VI Semiconductor Nanocrystals in Noncoordinating Solvents: Tunable Reactivity of Monomers. *Angew. Chem., Int. Ed.* **2002**, *41*, 2368–2371.
37. Bullen, C. R.; Mulvaney, P. Nucleation and Growth Kinetics of CdSe Nanocrystals in Octadecene. *Nano Lett.* **2004**, *4*, 2303–2307.
38. van Embden, J.; Mulvaney, P. Nucleation and Growth of CdSe Nanocrystals in a Binary Ligand System. *Langmuir* **2005**, *21*, 10226–10233.
39. Owen, J. S.; Chan, E. M.; Liu, H.; Alivisatos, A. P. Precursor Conversion Kinetics and the Nucleation of Cadmium Selenide Nanocrystals. *J. Am. Chem. Soc.* **2010**, *132*, 18206–18213.
40. Chan, E. M.; Xu, C. X.; Mao, A. W.; Han, G.; Owen, J. S.; Cohen, B. E.; Milliron, D. J. Reproducible, High-Throughput Synthesis of Colloidal Nanocrystals for Optimization in Multidimensional Parameter Space. *Nano Lett.* **2010**, *10*, 1874–1885.
41. Xie, R. G.; Li, Z.; Peng, X. G. Nucleation Kinetics vs Chemical Kinetics in the Initial Formation of Semiconductor Nanocrystals. *J. Am. Chem. Soc.* **2009**, *131*, 15457–15466.
42. Steckel, J. S.; Yen, B. K. H.; Oertel, D. C.; Bawendi, M. G. On the Mechanism of Lead Chalcogenide Nanocrystal Formation. *J. Am. Chem. Soc.* **2006**, *128*, 13032–13033.
43. Liu, H. T.; Owen, J. S.; Alivisatos, A. P. Mechanistic Study of Precursor Evolution in Colloidal Group II—VI Semiconductor Nanocrystal Synthesis. *J. Am. Chem. Soc.* **2007**, *129*, 305–312.
44. Rempel, J. Y.; Bawendi, M. G.; Jensen, K. F. Insights into the Kinetics of Semiconductor Nanocrystal Nucleation and Growth. *J. Am. Chem. Soc.* **2009**, *131*, 4479–4489.
45. Capek, R. K.; Lambert, K.; Dorfs, D.; Smet, P. F.; Poelman, D.; Eychmüller, A.; Hens, Z. Synthesis of Extremely Small CdSe and Bright Blue Luminescent CdSe/ZnS Nanoparticles by a Prefocused Hot-Injection Approach. *Chem. Mater.* **2009**, *21*, 1743–1749.
46. Sugimoto, T. Preparation of Monodispersed Colloidal Particles. *Adv. Colloid Interface Sci.* **1987**, *28*, 65–108.
47. Kwon, S. G.; Piao, Y.; Park, J.; Angappane, S.; Jo, Y.; Hwang, N.-M.; Park, J.-G.; Hyeon, T. Kinetics of Monodisperse Iron Oxide Nanocrystal Formation by "Heating-Up" Process. *J. Am. Chem. Soc.* **2007**, *129*, 12571–12584.
48. Talapin, D. V.; Rogach, A. L.; Haase, M.; Weller, H. Evolution of an Ensemble of Nanoparticles in a Colloidal Solution: Theoretical Study. *J. Phys. Chem. B* **2001**, *105*, 12278–12285.

49. Clark, M. D.; Kumar, S. K.; Owen, J. S.; Chan, E. M. Focusing Nanocrystal Size Distributions via Production Control. *Nano Lett.* **2011**, *11*, 1976–1980.
50. Joo, J.; Pietryga, J. M.; McGuire, J. A.; Jeon, S.-H.; Williams, D. J.; Wang, H.-L.; Klimov, V. I. A Reduction Pathway in the Synthesis of PbSe Nanocrystal Quantum Dots. *J. Am. Chem. Soc.* **2009**, *131*, 10620–10628.
51. Capek, R. K.; Moreels, I.; Lambert, K.; De Muynck, D.; Zhao, Q.; Van Tomme, A.; Vanhaecke, F.; Hens, Z. Optical Properties of Zincblende Cadmium Selenide Quantum Dots. *J. Phys. Chem. C* **2010**, *114*, 6371–6376.
52. Yu, W. W.; Qu, L. H.; Guo, W. Z.; Peng, X. G. Experimental Determination of the Extinction Coefficient of CdTe, CdSe, and CdS Nanocrystals. *Chem. Mater.* **2003**, *15*, 2854–2860.
53. Hens, Z.; Moreels, I.; Martins, J. C. In Situ H-1 NMR Study on the Trioctylphosphine Oxide Capping of Colloidal InP Nanocrystals. *ChemPhysChem* **2005**, *6*, 2578–2584.
54. Moreels, I.; Fritzinger, B.; Martins, J. C.; Hens, Z. Surface Chemistry of Colloidal PbSe Nanocrystals. *J. Am. Chem. Soc.* **2008**, *130*, 15081–15086.